Effects of Heteroatoms on Aromatic $\pi-\pi$ Interactions: Benzene−Pyridine and Pyridine Dimer

Edward G. Hohenstein[†] and C. David Sherrill*[,†,‡]

Center for Computational Molecular Science and Technology, School of Chemistry and Biochemistry, Georgia Institute of Technology, Atlanta, Georgia 30332-0400, and College of Computing, Georgia Institute of Technology, Atlanta, Georgia 30332-0280

Received: October 13, 2008; Revised Manuscript Received: November 20, 2008

Heteroatoms are found in many noncovalent complexes which are of biological importance. The effect of heteroatoms on $\pi-\pi$ interactions is assessed via highly accurate quantum chemical computations for the two simplest cases of interactions between aromatic molecules containing heteroatoms, namely, benzene−pyridine and pyridine dimer. Benchmark quality estimated coupled-cluster through perturbative triples [CCSD(T)] binding energies are computed near the complete basis set limit. Comparisons to the benzene dimer are made to determine the contributions from heteroatoms. The presence of a heteroatom reduces the spatial extent of the π-electron cloud and polarizability of pyridine as compared to benzene. As a result, the magnitude of the dispersion, exchange, and induction interactions in benzene−pyridine and pyridine dimer is generally reduced as compared to those for the benzene dimer. Benzene−pyridine and pyridine dimer bind more strongly than the benzene dimer in several configurations, and in contrast to the benzene dimer, parallel-displaced configurations can be significantly preferred over T-shaped configurations. Hydrogens para to a heteroatom are more effective "π-hydrogen bond" donors, but aromatic rings with heteroatoms are worse "π-hydrogen bond" acceptors.

1. Introduction

Aromatic $\pi-\pi$ interactions contribute to the stability of DNA and proteins,[1−3] to drug binding, and to the structure and lattice energies of organic crystals.[4,5] In an effort to better understand these interactions, the benzene dimer[6−14] and substituted benzene dimers[15−33] have been studied extensively as model systems for aromatic $\pi-\pi$ interactions. Surprisingly, however, relatively little theoretical work has attempted to understand the general and fundamental question of how heteroatoms influence $\pi-\pi$ interactions. Nitrogen heteroatoms are present in nucleic acid bases and presumably they influence the stacking energies between bases and hence the structure of DNA and RNA.[3,34,35] Additionally, the study of intercalation phenomena could benefit from an understanding of how heteroatoms will affect aromatic $\pi-\pi$ interactions.[3]

Bimolecular complexes involving pyridine have been studied theoretically by several groups. Some of the first work studying the pyridine dimer was conducted by Megiel et al.;[36] the dependence of the chemical shift of the pyridine nitrogen was studied as a function of pyridine concentration in *n*-heptane, and hydrogen-bonded configurations of the pyridine dimer were examined with Hartree−Fock and density functional theory (DFT). Optimized geometries and binding energies of the pyridine dimer were computed by Piacenza and Grimme using dispersion corrected density functional theory (DFT-D), second-order Møller−Plesset perturbation theory (MP2), and spin-component-scaled MP2 methods.[37] Binding energies for pyridine dimers and trimers were also computed by Mishra and Sathyamurthy at the MP2/6-311++G** level of theory.[38] Geerlings and co-workers studied complexes of pyridine, pyrimidine, and imidazole with substituted benzenes at the MP2/6-31G*(0.25) level of theory to examine the effect of substitution on binding energies and the H-bonding ability of the nitrogen lone pairs.[39] Tsuzuki et al.[40] have examined benzene−pyridine at a high level of theory as part of a study on interactions between benzene and pyridinium cations. However, relatively little work has sought to systematically explore the fundamental question of how heteroatoms affect $\pi-\pi$ interactions. As this article was being prepared, two additional relevant studies were published. Tschumper and co-workers have examined complexes involving benzene, 1,3,5-triazine, cyanogen, and diacetylene.[41] Wang and Hobza[42] have presented high-quality interaction energies for selected configurations of benzene with isoelectronic nitrogen-containing heterocycles.

In this study, quantum chemical methods are used to compute benchmark quality binding energies and potential energy curves for benzene−pyridine and the pyridine dimer. Previous works have presented fully optimized geometries for these complexes,[37,40,42] which are important for understanding their spectroscopy. However, our present interest is not the spectroscopy of these clusters, but rather how heteroatoms tune $\pi-\pi$ interactions across the energy landscape. Such information can be valuable because heteroatom-containing $\pi-\pi$ interactions may occur in a wide variety of geometries in complex systems such as biopolymers. Because full six-dimensional intermolecular potential surfaces are difficult to visualize and compute, our strategy here is to compare several interesting configurations of the pyridine dimer to corresponding configurations in benzene−pyridine and the benzene dimer to ascertain the heteroatom effect. In addition, we plot selected potential energy curves.

To better understand the nature of heteroatom-influenced $\pi-\pi$ interactions, it is also useful to analyze the interaction energy

* Corresponding author.
[†] Center for Computational Molecular Science and Technology, School of Chemistry and Biochemistry.
[‡] College of Computing.

10.1021/jp809062x CCC: $40.75
Published on Web 01/08/2009

in terms of electrostatic, induction, dispersion, and exchange-repulsion components. Previous work on benzene−pyridine has considered such an analysis by using approximate energy decomposition schemes.[40] Here we employ the rigorous symmetry-adapted perturbation theory (SAPT)[43,44] to analyze the sandwich, T-shaped, and parallel-displaced configurations of both benzene−pyridine and pyridine dimer, and we find that SAPT leads to somewhat different conclusions than previous analyses.

2. Theoretical Methods

Single-point energy computations were performed by using second-order perturbation theory (MP2) as well as coupled-cluster with singles and doubles including perturbative triples [CCSD(T)].[45] These methods were used with Dunning's aug-cc-pVDZ, aug-cc-pVTZ, and aug-cc-pVQZ basis sets.[46,47] In addition, the spin-component-scaled second-order perturbation theory (SCS-MP2) method of Grimme was used to analyze parallel-displaced configurations.[48] Within each complex, the monomer geometries were held rigid as the intermonomer distance was varied. Experimental geometries for each monomer were used. The benzene monomer geometry is that recommended by Gauss and Stanton: $r_{CC} = 1.3915$ Å and $r_{CH} = 1.0800$ Å.[49] The monomer geometry of pyridine used in this study is that reported by Innes et al.[50] The sandwich and T-shaped benzene dimer curves were obtained in a separate work.[51]

To correct for basis set superposition error, the Boys−Bernardi counterpoise correction scheme was employed for all energy computations.[52] Large-basis CCSD(T) results are estimated by using an additive scheme that adds a "coupled-cluster correction", $\Delta\mathrm{CCSD(T)} = E_{\mathrm{CCSD(T)}}^{\text{small-basis}} - E_{\mathrm{MP2}}^{\text{small-basis}}$, to a large-basis MP2 result: $E_{\mathrm{CCSD(T)}}^{\text{large-basis}} \approx E_{\mathrm{MP2}}^{\text{large-basis}} + \Delta\mathrm{CCSD(T)}$. Previous work suggests that this correction is fairly well converged with the aug-cc-pVDZ basis set,[12] although more recent work suggests that the size of the correction might grow slightly if larger basis sets could be employed.[53]

Dunning's correlation consistent basis sets have been shown to systematically approach the complete-basis-set (CBS) limit; this was exploited to obtain estimates of the MP2/CBS binding energies by using the two-point extrapolation scheme of Halkier et al.[54] with aug-cc-pVTZ and aug-cc-pVQZ basis sets. All CCSD(T) and MP2 computations were performed with the core electrons frozen by using the PSI 3.3 and MOLPRO programs.[55,56] A natural population analysis of benzene and pyridine for the Hartree−Fock/6-311++G** wave function was performed with Jaguar.[57]

Energy component analysis was performed by using symmetry-adapted perturbation theory (SAPT).[43,44] The terms computed in this work were second order or lower with respect to the intermolecular correlation operator, thus designating this truncation of SAPT theory SAPT2. For the purpose of analysis in this work, each of these terms are categorized as below,[19] where the individual terms are defined as in refs 43 and 44. The sum of all these terms leads to the SAPT2 binding energy for the dimer.

$$E_{\text{electrostatic}} = E_{\text{elst}}^{(10)} + E_{\text{elst,resp}}^{(12)} \quad (1)$$

$$E_{\text{exchange}} = E_{\text{exch}}^{(10)} + E_{\text{exch}}^{(11)} + E_{\text{exch}}^{(12)} \quad (2)$$

$$E_{\text{induction}} = E_{\text{ind,resp}}^{(20)} + E_{\text{exch-ind,resp}}^{(20)} + \delta E_{\text{ind,resp}}^{(\text{HF})} + {}^{t}E_{\text{ind}}^{(22)} + {}^{t}E_{\text{exch-ind}}^{(22)} \quad (3)$$

$$E_{\text{dispersion}} = E_{\text{disp}}^{(20)} + E_{\text{exch-disp}}^{(20)} \quad (4)$$

All SAPT2 computations were performed with the SAPT2006 program.[58] These computations were performed with the aug-cc-pVDZ′ basis set, which consists of the cc-pVDZ basis set with the diffuse s and p functions of aug-cc-pVDZ added to non-hydrogen atoms. In our experience, the SAPT2/aug-cc-pVDZ′ results are good approximations to large-basis CCSD(T) results through a favorable cancelation of errors.[12]

3. Results and Discussion

The configurations of benzene dimer, benzene−pyridine, and pyridine dimer studied here fall into three categories: sandwich (Figure 1), T-shaped (Figure 2), and parallel-displaced (Figure 3). For all configurations, the monomers were aligned based on the geometric centers of their rings. The vertical intermonomer separation in all cases was measured from these centers and is denoted as R. For the parallel-displaced configurations, the horizontal displacement is labeled H. The pyridine dimer has the most possible unique configurations, and because of this, the focus of this work was on the configurations that represented extremes for pyridine dimer: placing the nitrogen atoms as close and as far away from one another as possible, and aligning the dipole moments in parallel and antiparallel arrangements. The analogous configurations for benzene−pyridine were also studied. Each of these configurations was compared to a similar configuration of benzene dimer. For convenience in the following discussion, we will frequently abbreviate pyridine as Py and benzene as Bz.

Potential energy curves were computed for sandwich configurations of benzene−pyridine and pyridine dimer at the estimated CCSD(T) complete basis set limit. These computations show $(Py)_2$ S2 to be the most favorable sandwich configuration, followed by Bz-Py S (see Table 1). With a binding energy of 2.95 kcal mol^{-1}, $(Py)_2$ S2 binds nearly twice as strongly as $(Bz)_2$ S. The least favorable configuration, and the only configuration to be less favorable than the benzene dimer sandwich configuration, is $(Py)_2$ S1.

Five of the more favorable T-shaped configurations of $(Py)_2$ or Bz-Py were analyzed at the estimated CCSD(T) CBS limit, and potential curves for the remaining T-shaped configurations from Figure 2 were computed at the estimated CCSD(T)/aug-cc-pVTZ level of theory. The most favorable T-shaped configuration was found to be Bz-Py T1, with $(Py)_2$ T3 being the second most favorable. These were the only two configurations found to be more favorable than $(Bz)_2$ T at the CCSD(T) CBS

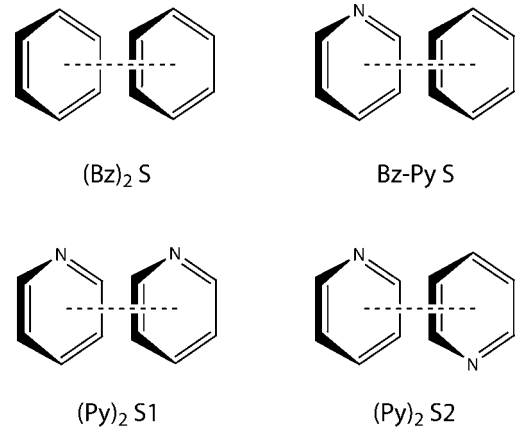

Figure 1. Sandwich and T-shaped configurations of benzene dimer, benzene−pyridine, and pyridine dimer.

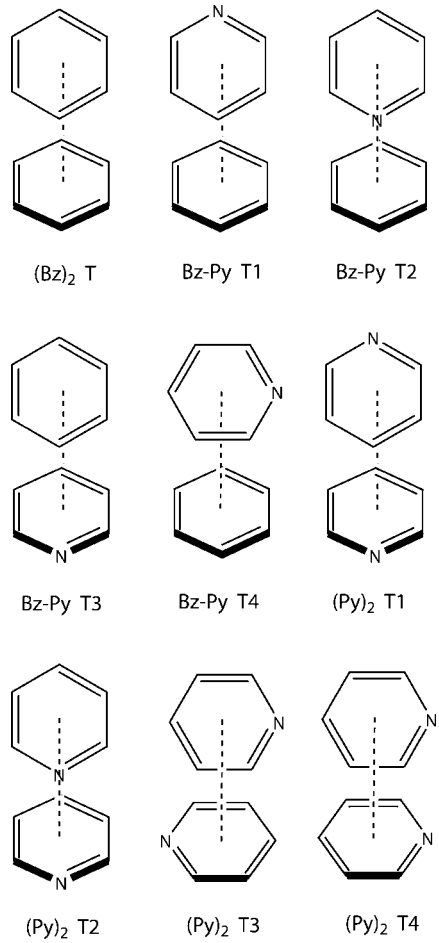

Figure 2. Sandwich and T-shaped configurations of benzene dimer, benzene−pyridine, and pyridine dimer.

limit. Configurations of the T2 type (with a nitrogen of one ring pointed down at the center of another ring) were found to be more weakly bound with a shorter optimized intermonomer separation.

Potential energy curves for the parallel-displaced configurations (Figure 3) were computed at vertical intermonomer separations of 3.2, 3.4, 3.5, 3.6, and 3.8 Å. Horizontal displacements as large as 6 Å were considered. The parallel-displaced configurations of type *a* exhibit displacements over a vertex, while configurations of type *b* were displaced over a bond. Because of the large number of single point energies required for a thorough analysis of these configurations, CCSD(T) curves proved to be far too costly. Instead, the less computationally expensive SCS-MP2 method was employed.[48] Figure 4 clearly shows that the SCS-MP2/aug-cc-pVTZ curves are an excellent estimate of the estimated CCSD(T)/aug-cc-pVTZ curves. The SCSN scaling of MP2[59] was tested but did not work as well as SCS-MP2 for these complexes. These favorable results allowed SCS-MP2 to be confidently applied to the remainder of the configurations. For completeness, SCS-MP2 can be compared to estimated CCSD(T) results with the aug-cc-pVTZ basis set for all complexes considered in this work (Table 1). SCS-MP2 performs well for sandwich configurations, further justifying its use for examining parallel-displaced complexes. The most favorable configuration of all those considered in this work is $(Py)_2$ P2b at $R = 3.4$ Å. This has a binding energy of 3.84 kcal mol^{-1} at the SCS-MP2/aug-cc-pVTZ level (Table 2). The most favorable benzene-pyridine configuration was Bz-Py P1a(−) at $R = 3.5$ Å with a binding energy of 3.23 kcal mol^{-1}.

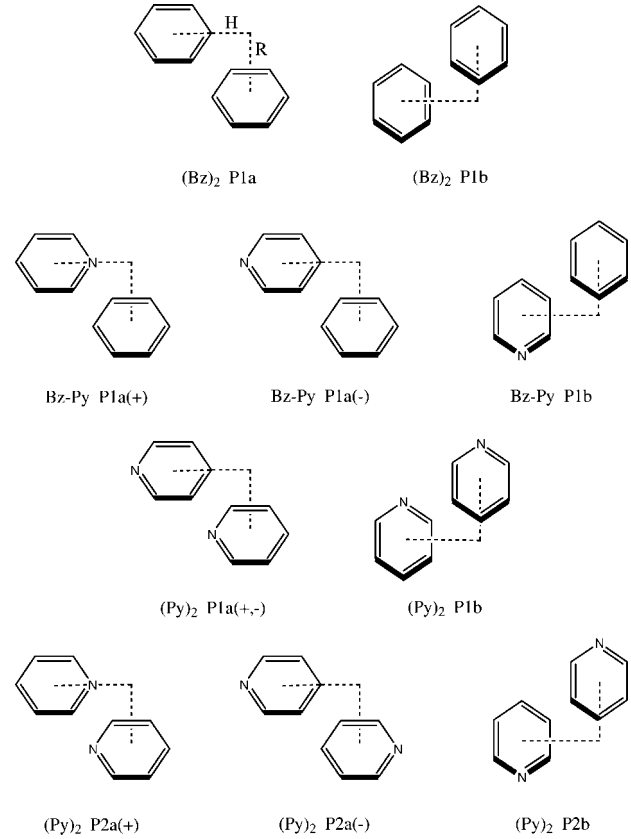

Figure 3. Parallel-displaced configurations of benzene dimer, benzene−pyridine, and pyridine dimer.

TABLE 1: Interactions Energies of Sandwich and T-Shaped Configurations of Benzene Dimer, Benzene−Pyridine, and Pyridine Dimer at Various Levels of Theory

	SCS-MP2/ aug-cc-pVTZ		est. CCSD(T)/ aug-cc-pVTZ		est. CCSD(T)/ CBS Limit	
	ΔE^a	R^b	ΔE^a	R^b	ΔE^a	R^b
$(Bz)_2$ S	−1.76	3.9	−1.64	3.9	−1.76	3.9
Bz-Py S	−2.19	3.8	−2.07	3.8	−2.22	3.8
$(Py)_2$ S1	−1.56	3.8	−1.48	3.9	−1.61	3.8
$(Py)_2$ S2	−2.88	3.7	−2.77	3.7	−2.95	3.7
$(Bz)_2$ T	−2.33	5.0	−2.59	4.9	−2.73	5.0
Bz-Py T1	−2.74	5.0	−3.02	5.0	−3.18	4.9
Bz-Py T2	−0.39	4.8	−0.64	4.7		
Bz-Py T3	−1.80	5.1	−2.08	5.0	−2.20	5.0
Bz-Py T4	−2.36	5.0	−2.61	5.0	−2.74	5.0
$(Py)_2$ T1	−2.02	5.1	−2.32	5.0	−2.46	5.0
$(Py)_2$ T2	−0.95	4.7	−1.23	4.6		
$(Py)_2$ T3	−2.55	5.0	−2.80	4.9	−2.95	4.9
$(Py)_2$ T4	−1.87	5.0	−2.15	5.0		

[a] CCSD(T) estimated CBS limit interaction energies in kcal mol^{-1}. [b] Intermonomer separation in Å.

The presence of nitrogen atoms in pyridine allows for the possibility of planar complexes with favorable CH···N interactions. In a previous work by Piacenza and Grimme,[37] a configuration of pyridine dimer with C_{2h} symmetry containing two CH···N interactions was examined. There are no analogous benzene dimer or benzene−pyridine configurations, and this configuration is the least significant for the $\pi-\pi$ interactions which are the focus of this work. Nevertheless, due to the magnitude of the favorable interactions within this complex and the importance of hydrogen bonded interactions in biological complexes, the hydrogen bonded pyridine dimer is interesting in its own right. A potential energy curve for this complex was

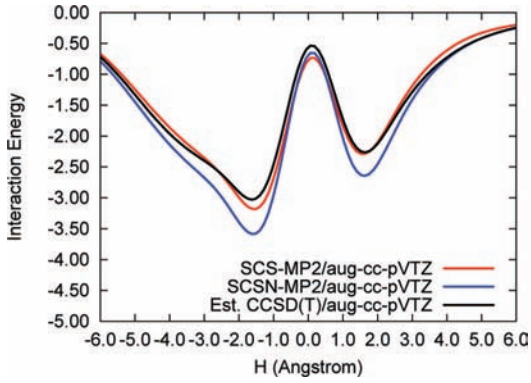

Figure 4. Comparison of Bz-Py P1a(+,−) potential energy curves computed with various methods. Interaction energies in kcal mol^{-1}.

TABLE 2: Interaction Energies of Parallel-Displaced Configurations of Benzene Dimer, Benzene−Pyridine, and Pyridine Dimer Computed at the SCS-MP2/aug-cc-pVTZ Level of Theory

	SCS-MP2/aug-cc-pVTZ		
	ΔE^a	R^b	H^b
$(Bz)_2$ P1a	−2.71	3.5	1.6
$(Bz)_2$ P1b	−2.70	3.5	1.6
Bz-Py P1a(+)	−2.36	3.5	1.4
Bz-Py P1a(−)	−3.23	3.5	1.6
Bz-Py P1b	−3.14	3.5	1.6
$(Py)_2$ P1a	−2.24	3.5	1.6
$(Py)_2$ P1b	−2.54	3.5	1.6
$(Py)_2$ P2a(+)	−2.78	3.5	1.4
$(Py)_2$ P2a(−)	−3.70	3.5	1.2
$(Py)_2$ P2b	−3.84	3.4	1.6

[a] SCS-MP2/aug-cc-pVTZ interaction energies in kcal mol^{-1}. [b] Distances given in Å.

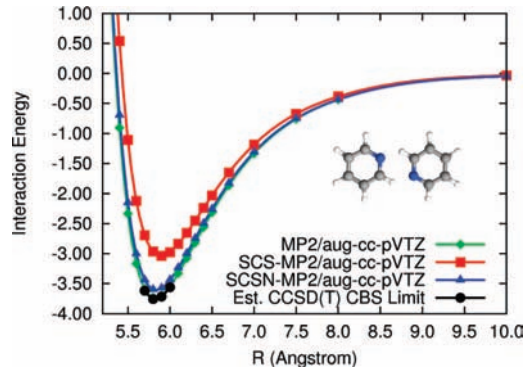

Figure 5. Potential energy curves for the hydrogen bonded pyridine dimer computed at the estimated CCSD(T)/aug-cc-pVTZ level of theory. Interaction energies in kcal mol^{-1}.

computed at the estimated CCSD(T)/aug-cc-pVTZ level of theory (Figure 5). This complex is bound by 3.56 kcal mol^{-1} at an intermonomer separation of 5.8 Å with CH···N hydrogen bond distances of 2.5 Å. SCS-MP2 and SCSN-MP2 were tested for this hydrogen bonded pyridine dimer: MP2 and SCSN-MP2 perform well, while SCS-MP2 significantly underestimates the magnitude of the attractive interaction. Using DFT-D, a much less computationally demanding technique than CCSD(T), Piacenza and Grimme report binding energies of 3.5−3.7 kcal mol^{-1} for the planar hydrogen bonded pyridine dimer.[37] These are in excellent agreement with our benchmark CCSD(T) results.

Sandwich Configurations. The most obvious difference in the intermolecular interactions of the $(Py)_2$ S1 and $(Py)_2$ S2 configurations is that they feature dipole−dipole interactions

TABLE 3: SAPT2 Results for Sandwich Configurations of Benzene Dimer, Benzene−Pyridine, and Pyridine Dimer[a]

	R^b	elst	ind	exch	disp	net disp[c]	SAPT2[d]
$(Bz)_2$ S	3.8	−0.477	−0.275	4.516	−5.682	−1.166	−1.917
Bz-Py S	3.8	−0.800	−0.257	3.999	−5.335	−1.336	−2.393
$(Py)_2$ S1	3.8	−0.049	−0.208	3.565	−4.999	−1.435	−1.691
$(Py)_2$ S2	3.8	−1.294	−0.245	3.488	−4.996	−1.508	−3.047

[a] Computations preformed with the aug-cc-pVDZ′ basis set. Energies in kcal mol^{-1} and distances in Å. [b] Intermonomer separation in Å. [c] Net dispersion is the sum of the exchange and dispersion components. [d] Total SAPT2 interaction energy.

with opposite signs. The $(Py)_2$ S1 configuration has an unfavorable dipole−dipole interaction because the dipoles are parallel, while $(Py)_2$ S2 has a favorable dipole−dipole interaction because the dipoles are antiparallel. In Bz-Py S, dipole−induced-dipole interactions are expected to contribute favorably to the binding energy. Note that all of these electrostatic interactions differ qualitatively from those in the benzene dimer, which lacks dipoles on the monomers; instead, the benzene dimer features quadrupole−quadrupole interactions. However, all of the sandwiches considered here, as well as the benzene dimer, do have in common favorable charge interpenetration terms due to an overlap of the π clouds.

Dispersion is also important in weakly bonded systems, and its magnitude can be related to the polarizability of the monomers. Pyridine is less polarizable than benzene.[60] This causes the dispersion interactions in complexes containing pyridine to be weaker than those containing benzene. On the other hand, the contraction of the π-electron cloud due to the heteroatom not only decreases the size of the favorable dispersion interactions, but also decreases unfavorable exchange-repulsion interactions. Predictions about the relative size of these two changes are difficult to make; analysis with SAPT2 proves invaluable for quantifying these effects.

The SAPT2 results for the sandwich configurations at a separation of 3.8 Å (Table 3) generally confirm the above qualitative predictions about the various contributions to the interaction energy. Note that SAPT2 provides the same energetic ordering of sandwich complexes as does CCSD(T) estimated at the CBS limit. The $(Py)_2$ S2 configuration is predicted to have the most favorable electrostatic interactions and the least amount of dispersion, exchange-repulsion, and induction. These results stem from the reduced polarizability of pyridine and the antiparallel alignment of the dipoles. As well as producing favorable electrostatic interactions, this alignment of the dipoles also maximizes separation of the electron density, thus lowering dispersion and exchange-repulsion. Each successive substitution of a pyridine for a benzene lowers the exchange-repulsion by

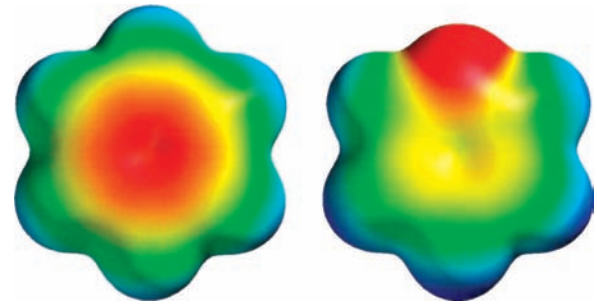

Figure 6. Electrostatic potential computed at the Hartree−Fock/6-31G* level of theory. The scale is −25 (red) to 25 (blue) kcal mol^{-1}. A benzene molecule is shown on the left, pyridine is on the right.

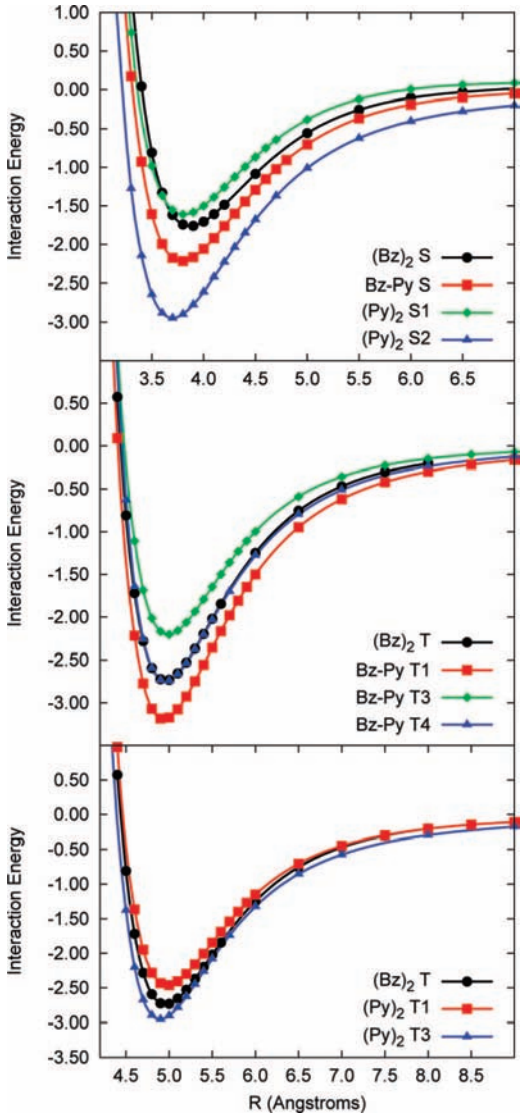

Figure 7. Potential energy curves for sandwich and T-shaped configurations computed at the estimated CCSD(T) CBS limit. Interaction energies in kcal mol^{-1}.

roughly 0.5 kcal mol^{-1}. However, the magnitude of the favorable dispersion interaction is reduced by only about 0.3 kcal mol^{-1} per pyridine monomer. Because of this, the sum of dispersion and exchange-repulsion ("net dispersion") tends to become more favorable as benzenes are replaced by pyridines. As expected, the $(Py)_2$ S1 configuration is much less favorable than $(Py)_2$ S2 or $(Bz)_2$ S because of the parallel alignment of dipoles; this is reflected in a much less attractive electrostatic interaction in this configuration. The Bz-Py S configuration has a somewhat more favorable electrostatic contribution than $(Bz)_2$ S, but less favorable than that due to the antiparallel dipoles of $(Py)_2$ S2. Perhaps surprisingly, the expected stabilization of Bz-Py S due to dipole−induced-dipole terms is not realized in the SAPT results; instead, the induction contribution for Bz-Py S is less attractive than in $(Bz)_2$ S. This unimportance of dipole−induced-dipole interactions has also been noted in substituted benzene dimers.[17,19]

Figure 7 shows the potential energy of the sandwich configurations as a function of the intermonomer separation. For all distances considered, the Bz-Py heterodimer energy lies in between those of the $(Bz)_2$ S and $(Py)_2$ S2 dimers, although the energy is somewhat closer to that of $(Bz)_2$ S. The $(Py)_2$ S1 configuration is the least favorable sandwich except at short distances (R < 3.5 Å) when it becomes slightly more favorable than $(Bz)_2$ S. This is due to the reduced spatial extent of the electron density for a pyridine monomer reducing the rate at which exchange-repulsion increases with decreasing intermonomer separation relative to $(Bz)_2$ S.

TABLE 4: SAPT2 Results for T-Shaped Configurations of Benzene Dimer, Benzene−Pyridine, and Pyridine Dimer[a]

	R^b	elst	ind	exch	disp	net disp[c]	SAPT2[d]
$(Bz)_2$ T	5.0	−1.753	−0.518	3.517	−3.730	−0.213	−2.484
Bz-Py T1	5.0	−2.118	−0.635	3.540	−3.696	−0.156	−2.909
Bz-Py T2	4.7	0.329	−0.616	3.381	−3.754	−0.372	−0.659
Bz-Py T3	5.0	−1.209	−0.399	3.271	−3.512	−0.241	−1.850
Bz-Py T4	5.0	−1.804	−0.485	3.209	−3.359	−0.150	−2.439
$(Py)_2$ T1	5.0	−1.391	−0.498	3.288	−3.477	−0.189	−2.078
$(Py)_2$ T2	4.7	−0.392	−0.536	3.171	−3.534	−0.363	−1.292
$(Py)_2$ T3	5.0	−1.780	−0.378	2.674	−3.106	−0.431	−2.589
$(Py)_2$ T4	5.0	−1.138	−0.383	2.776	−3.124	−0.348	−1.869

[a] Computations preformed with the aug-cc-pVDZ′ basis set. Energies in kcal mol^{-1} and distances in Å. [b] Intermonomer separation in Å. [c] Net dispersion is the sum of the exchange and dispersion components. [d] Total SAPT2 interaction energy.

T-Shaped Configurations. The behavior of the T-shaped configurations containing pyridine monomers can be understood by examining how the interactions that stabilize the T-shaped benzene dimer are changed by the introduction of a heteroatom. As demonstrated by SAPT analysis (Table 4), the dominant stabilizing interaction in most of the T-shaped configurations is electrostatic; exchange-repulsion and dispersion terms are also large, but they tend to cancel, so their sum (net dispersion) is relatively small. The favorable electrostatic interaction can be rationalized by considering the attraction that will result between the negative π cloud on one ring and the positive charge on the hydrogen pointed toward it. In pyridine, the nitrogen atom pulls electron density away from the hydrogen para to it, increasing that hydrogen's positive charge relative to its value in benzene, making pyridine more effective as a "π-hydrogen bond" donor. However, because the presence of this nitrogen also distorts the π-electron cloud by pulling electron density away from the center of the ring and toward the nitrogen (see Figure 6), one might expect that this makes pyridine somewhat less effective than benzene as a "π-hydrogen bond" acceptor; indeed, Bz-Py T3 is less favorable than $(Bz)_2$ T, and $(Py)_2$ T1 is less favorable than Bz-Py T1. The Bz-Py T1 configuration should be the most favorable of those considered, and this conclusion is supported by the estimated CCSD(T) CBS limit potential energy curves (see Table 1 and Figure 7). Because $(Py)_2$ T1 is not as strongly bound as $(Bz)_2$ T, it appears that nitrogen heteroatoms have a larger unfavorable effect on "π-hydrogen bond" accepting ability than they have a favorable effect on "π-hydrogen bond" donating ability. The weak binding in the Bz-Py T2 and $(Py)_2$ T2 complexes occurs because the electrostatic contribution is much less favorable or even unfavorable as the negative charge on nitrogen points down at the negative π cloud below (see Table 1 and Figure 8). These complexes remain weakly bound because of favorable induction and dispersion contributions. The minimum energy geometries of these two complexes have shorter intermonomer separations than the other T-shaped complexes.

In complexes $(Py)_2$ T3 and $(Py)_2$ T4, the top pyridine is rotated 90°, leading to significant contributions from dipole−dipole interactions. We also examined a similar Bz-Py configuration, T4. The direct interaction between a single hydrogen with the π-electron cloud below it is replaced by a less direct interaction of two hydrogens with the π cloud. The estimated CCSD(T)

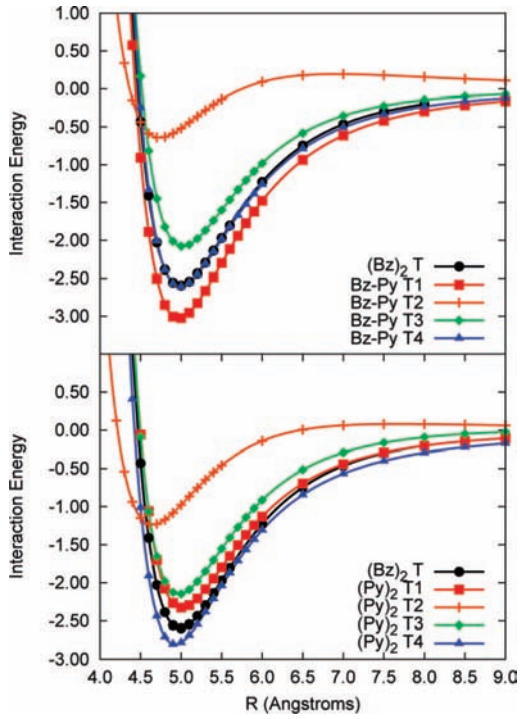

Figure 8. Potential energy curves for T-shaped configurations computed at the estimated CCSD(T)/aug-cc-pVTZ level of theory. Interaction energies in kcal mol^{-1}.

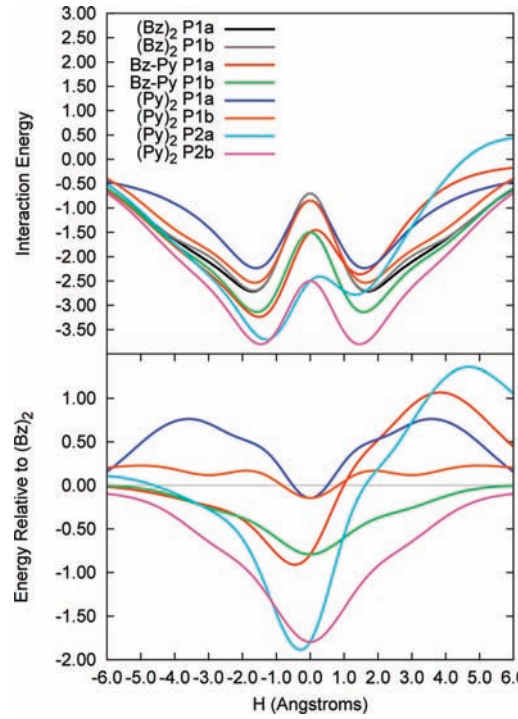

Figure 9. Potential energy curves for parallel-displaced configurations computed at a vertical displacement of 3.5 Å. Potential curves relative to $(Bz)_2$ P1a for *a* configurations or $(Bz)_2$ P1b for *b* configurations are also shown. Interaction energies in kcal mol^{-1}.

CBS limit potential energy curves show $(Py)_2$ T3 to be the most favorable of these three configurations, which would be expected because this configuration features antiparallel dipoles. This is the most favorable T-shaped pyridine dimer considered, and the only one that binds more strongly than $(Bz)_2$ T. Bz-Py T4 binds more weakly than the benzene dimer by a small amount. The least favorable complex is of course $(Py)_2$ T4, in which the dipoles are parallel.

To quantify the change in the positive charge on the interacting hydrogen, natural population analysis charges were computed for benzene and pyridine with a Hartree−Fock/6-311++G** wave function. The para carbon and hydrogen in pyridine become more positive relative to benzene. This causes the electrostatic interaction between the para position and the π cloud of the benzene monomer below it to be larger in Bz-Py T1 than in $(Bz)_2$ T. As shown in Table 4, the sum of dispersion and exchange-repulsion is comparable to the size of the electrostatic contribution only in the case of the weakly bound Bz-Py T2 and $(Py)_2$ T2 complexes; for all other configurations, the electrostatic contribution dominates and is stabilizing by 1 kcal mol^{-1} or more. The SAPT2 computations show that inductive effects are also an important factor stabilizing the T-shaped complexes. This contribution is stabilizing by 0.52 kcal mol^{-1} in the benzene dimer due to the quadrupole induced-multipole interactions, and perhaps surprisingly it remains close to this size in all of the Bz-Py and $(Py)_2$ T-shaped complexes considered, even though pyridine features a dipole rather than a quadrupole moment. Because pyridine is less polarizable than benzene, configurations in which the lower monomer is pyridine tend to have less favorable induction contributions than the benzene dimer. Induction is enhanced in the two Bz-Py T-shaped configurations (T1 and T2) in which the dipole of pyridine is parallel to the C_6 axis of the benzene below it.

Parallel-Displaced Configurations. The parallel-displaced configurations were analyzed at the SCS-MP2/aug-cc-pVTZ level of theory. The sign of the horizontal displacement is shown by (+) and (−) for the cases that are not symmetric with respect to horizontal displacements away from the sandwich configuration; in all of the "edgewise" displaced configurations, labeled *b*, the geometries are symmetric with respect to the horizontal displacement. The dipole−dipole interactions and the interplay between dispersion and exchange-repulsion seen in sandwich configurations are also observed in the parallel-displaced complexes. The interactions between hydrogen atoms and π-electron clouds important in the T-shaped configurations are also seen here. Due to the complicated interplay between these various contributions, SAPT2 analysis and potential energy curves relative to benzene dimer are essential to understanding the behavior of these interactions.

The potential energy curves for the parallel-displaced configurations at a vertical separation of 3.5 Å are shown in Figure 9. The most favorable geometries found in this work and their corresponding interaction energies are contained in Table 2. The most favorable of the complexes examined is $(Py)_2$ P2b; this is the $(Py)_2$ S2 geometry displaced "edgewise". $(Py)_2$ P2a(−) lies only 0.14 kcal mol^{-1} above $(Py)_2$ P2b; both of these complexes contain antiparallel dipoles. The next most favorable complex is Bz-Py P1a(−), and also in this case the Bz-Py P1b complex is nearly isoenergetic, differing by only 0.09 kcal mol^{-1}. In this case the "edgewise" displacement is not as favorable as the "over vertex" displacement. As a result of the higher symmetry in benzene compared to pyridine, the difference between displacements over a vertex or over an edge is even smaller in the benzene dimer, merely 0.01 kcal mol^{-1} at the SCS-MP2/aug-cc-pVTZ level of theory. The most favorable pyridine-containing parallel-displaced complexes are bound more strongly than the benzene dimer. Not surprisingly, the $(Py)_2$ P1a and $(Py)_2$ P1b dimers are the least favorable as a result of their parallel dipoles. With regard to the conclusion that the Bz-Py P1a(−) configuration is the most favorable benzene−pyridine complex, the data

TABLE 5: SAPT2 Results for Parallel-Displaced Configurations of Benzene Dimer, Benzene−Pyridine, and Pyridine Dimer[a]

	R^b	H^c	elst	ind	exch	disp	net disp[d]	SAPT2[e]
$(Bz)_2$ P1a	3.4	1.6	−2.774	−0.882	8.584	−7.879	0.705	−2.952
$(Bz)_2$ P1b	3.4	1.6	−2.805	−0.912	8.677	−7.883	0.795	−2.922
Bz-Py P1a(+)	3.4	1.6	−1.905	−0.733	7.244	−7.156	0.088	−2.550
Bz-Py P1a(−)	3.4	1.6	−3.235	−0.853	8.248	−7.587	0.661	−3.427
Bz-Py P1b	3.4	1.6	−2.948	−0.807	7.768	−7.383	0.386	−3.369
$(Py)_2$ P1a	3.4	1.6	−1.742	−0.682	6.969	−6.897	0.072	−2.353
$(Py)_2$ P1b	3.4	1.6	−2.039	−0.663	7.008	−6.927	0.081	−2.621
$(Py)_2$ P2a(+)	3.4	1.6	−1.781	−0.655	5.904	−6.456	−0.553	−2.988
$(Py)_2$ P2a(−)	3.4	1.6	−3.538	−0.786	7.926	−7.302	0.624	−3.701
$(Py)_2$ P2b	3.4	1.6	−3.258	−0.703	6.851	−6.894	−0.043	−4.004

[a] Computations preformed with the aug-cc-pVDZ′ basis set. Energies in kcal mol^{-1} and distances in Å. [b] Vertical separation in Å. [c] Horizontal separation in Å. [d] Net dispersion is the sum of the exchange and dispersion components. [e] Total SAPT2 interaction energy.

reported in this work agree with those of Tsuzuki et al.[40] Tsuzuki et al. report estimated CCSD(T) CBS limit binding energies of 3.04 and 2.22 kcal mol^{-1} for complexes very similar to our $(Py)_2$ P2a(−) and $(Py)_2$ P2a(+) configurations, respectively. This is in good agreement with the less computationally demanding SCS-MP2/aug-cc-pVTZ binding energies reported in this work of 3.23 and 2.36 kcal mol^{-1}, respectively.

The parallel-displaced complexes pass through sandwich configurations at $H = 0$. As can be seen in Figure 9, all of the pyridine-containing complexes are more favorable than the benzene dimer at $H = 0$ Å for a vertical distance of $R = 3.5$ Å (although the $(Py)_2$ P1 configurations are less favorable than benzene dimer at larger vertical separations due to the parallel pyridine dipoles). This is likely due to the contracted π-electron clouds seen in pyridine monomers. As discussed above, the contraction of these clouds leads to a reduction in exchange-repulsion relative to benzene dimer. In all of the complexes except $(Py)_2$ P1, there is also an increased electrostatic attraction. The "edgewise" displaced Bz-Py P1b and $(Py)_2$ P2b complexes remain more favorable than benzene dimer for the entire range of horizontal displacements examined. The Bz-Py P1a(+) and $(Py)_2$ P2a(+) complexes become less favorable than the benzene dimer as the nitrogen in the pyridine monomers begins interacting with the π-electron cloud of the other monomer. The $(Py)_2$ P1a and $(Py)_2$ P1b dimers become less favorable than the benzene dimer once the horizontal displacement increases sufficiently to lessen the importance of the reduced exchange-repulsion. Although these complexes remain less favorable than the benzene dimer for all horizontal displacements studied past the sandwich-like configurations, one can infer from the slope of the $(Py)_2$ P1a potential energy curve that it will become more favorable than the benzene dimer at larger horizontal displacements. This is likely due to slightly more favorable electrostatic interactions at large separations.

The SAPT2 decomposition of the interaction energies within these parallel-displaced complexes at a vertical separation of 3.4 Å and horizontal separation of 1.6 Å is presented in Table 5. The distance between ring centers at this displacement is comparable to that examined for the sandwich configurations (roughly 3.76 Å compared to 3.8 Å). The electrostatic and induction energies play a major role in the binding of these complexes. The net dispersion terms computed here are all repulsive for these complexes except for $(Py)_2$ P2a(+) and $(Py)_2$ P2b, although this may be different at other geometries. Both electrostatics and net dispersion can change significantly among the different complexes and orientations considered. The orientation of the dipoles is obviously important for the electrostatic interactions. However, the orientation of the pyridine monomers can also strongly influence the exchange-repulsion and dispersion terms. The induction terms, which depend on polarizability, are weakly affected by heteroatoms in parallel-displaced complexes, decreasing by about 0.1−0.2 kcal mol^{-1} compared to their value in the benzene dimer. At the geometry considered, the electrostatic term is larger than induction or net dispersion for the parallel-displaced configurations.

TABLE 6: Energy Component Analysis for Optimized Benzene−Pyridine Complexes for the Present Results with SAPT2 and Literature Results (from ref 40) in Parentheses[a]

	elst	ind	exch	disp	net disp[c]	ΔE[d]
Bz-Py P1a(+)	−1.012	−0.503	4.915	−6.000	−1.085	−2.599
	(0.99)	(−0.21)	(2.85)	(−5.84)	(−2.99)	(−2.22)
Bz-Py P1a(−)	−2.497	−0.698	6.472	−6.807	−0.334	−3.529
	(0.39)	(−0.22)	(3.27)	(−6.48)	(−3.21)	(−3.04)
Bz-Py T1	−1.882	−0.555	2.858	−3.343	−0.485	−2.922
	(−1.01)	(−0.20)	(1.26)	(−2.86)	(−1.60)	(−2.81)
Bz-Py T3	−1.382	−0.328	2.227	−3.074	−0.847	−2.557
	(−0.57)	(−0.08)	(0.88)	(−2.80)	(−1.92)	(−2.57)
Bz-Py T4	−2.003	−0.523	3.177	−3.626	−0.449	−2.976
	(−0.96)	(−0.19)	(1.60)	(−3.31)	(−1.71)	(−2.87)

[a] Energies in kcal mol^{-1}. SAPT2 Computations preformed with the aug-cc-pVDZ′ basis set with geometries reported by Tsuzuki et al.[40] [b] Decomposition performed by Tsuzuki et al.[40] [c] Net dispersion is the sum of the exchange and dispersion components. [d] Total interaction energy.

In a recent work by Tsuzuki et al.,[40] the interaction energy of parallel-displaced benzene−pyridine is decomposed into its physically relevant components, but with significantly different results than we present in this work using SAPT2. Those authors conclude that parallel-displaced pyridine−benzene complexes are bound primarily by net dispersion interactions. Although we concur that dispersion is the largest single stabilizing factor, our SAPT2 results suggest that net dispersion (the sum of dispersion and exchange-repulsion) is generally less important than electrostatics in these configurations. To examine this discrepancy, we performed a decomposition of the interaction energies for the geometries reported in Tsuzuki et al.[40] using SAPT2. The results are presented in Table 6. For the Bz-Py P1a geometries, the most striking difference is seen in the electrostatic contributions to the interaction. Our quantum mechanically based SAPT2 results predict electrostatic interactions to be a major factor stabilizing these complexes, while the decomposition from Tsuzuki et al. predicts that electrostatic interactions destabilize these complexes. This discrepancy results because Tsuzuki et al. used distributed multipoles to compute the electrostatic interaction. This procedure does not account for the favorable electrostatic interactions originating from the interpenetration of π-electrons, an effect that has been shown to be important for the stabilization of the benzene dimer.[19] The lower exchange energies obtained by Tsuzuki et al. are a direct result of the method used for the computation of the electrostatic interaction because the exchange energy was reported as the remainder of the interaction energy after dispersion, electrostatic, and induction energy had been computed explicitly. For completeness, we also used SAPT2 to examine the T-shaped complexes reported by Tsuzuki et al. As would be expected, the electrostatic interactions in the T-shaped complexes are described fairly well by the multipole analysis.

4. Conclusions

The parallel-displaced configurations of benzene−pyridine and pyridine dimer were the most favorable complexes studied in this work. In the case of the benzene dimer, the T-shaped and parallel-displaced configurations are nearly isoenergetic; by substituting nitrogen atoms (and consequently introducing dipole moments), the parallel-displaced configurations become favored. $(Py)_2$ P2b and Bz-Py P1a(−) were the most favorable configurations found for the pyridine dimer and benzene−pyridine complex, respectively. The most favorable benzene−pyridine complex was found to bind more strongly than benzene dimer by roughly 0.5 kcal mol^{-1}. The most favorable pyridine dimer was found to bind about 1 kcal mol^{-1} more strongly than benzene dimer. The intermonomer separation for the minimum energy structures of each configuration of benzene−pyridine and pyridine dimer did not change substantially relative to benzene dimer.

The substitution of a nitrogen atom into a benzene molecule creates a dipole in the molecule, reduces its polarizability, and reduces the spatial extent of the electron density. The presence of a heteroatom in pyridine makes the electrostatic interactions within pyridine-containing dimers much more sensitive to the orientation of the monomers. In general, the substitution of benzene monomers in benzene dimer with pyridine molecules will reduce the magnitude of the dispersion and induction interactions as a result of the reduced polarizability of pyridine. Similarly, the reduced spatial extent of the π-electron cloud in a pyridine molecule leads to reduced exchange-repulsion. These general trends observed here can be expected to persist in larger and more complex heteroatom-containing π systems.

For sandwich and parallel-displaced configurations, pyridine monomers cause dipole−induced-dipole interactions in benzene−pyridine and dipole−dipole interactions in pyridine dimer. The former is found to be relatively unimportant, while the latter is very important and can lead to more favorable or less favorable electrostatic interactions, depending on the configuration. The other important considerations, stemming from the decreased polarizability and reduced spatial extent of the electron density, are a reduction in the magnitude of the dispersion and exchange-repulsion energies relative to benzene dimer. Because the exchange-repulsion and dispersion terms are of opposite sign but with roughly equal magnitude, it is convenient to consider their sum, "net dispersion". The electrostatic and net dispersion interactions both play an important role in the interaction energy of the sandwich configurations. Limited SAPT2 analysis at selected geometries suggests that the electrostatic term tends to dominate the interaction energy near the equilibrium geometries of parallel-displaced configurations; in addition, the most strongly bound parallel-displaced pyridine-containing complexes studied in this work had electrostatic interactions that were much more favorable than the complexes which were bound more weakly. Generally speaking, electrostatics are also the dominant stabilizing factor in the T-shaped complexes, although there are also favorable induction and net dispersion contributions; in the $(Bz)_2$ T, Bz-Py T1, Bz-Py T3, and $(Py)_2$ T1 complexes the electrostatic attraction is related to what might be called a "π-hydrogen bond". For Bz-Py T4 and $(Py)_2$ T3 the favorable electrostatics originate from dipole effects. The less favorable Bz-Py T2, $(Py)_2$ T2, and $(Py)_2$ T4 complexes do not contain either the "π-hydrogen bonds" or stabilizing dipole effects. In all the configurations considered, there were benzene−pyridine and pyridine dimer complexes found that were more favorable than the analogous benzene dimer complex.

Previous work had indicated that parallel-displaced benzene−pyridine complexes are bound primarily due to dispersion effects. Our SAPT-based analysis indicates that dispersion is a major stabilizing force, but it is mostly canceled be exchange-repulsion. The sum of these two terms is usually repulsive at the near-equilibrium geometries considered. Electrostatic interactions are very important and are significantly stabilizing according to the quantum-mechanical SAPT method, which can capture charge interpenetration effects neglected in a multipole analysis.

Acknowledgment. This material is based upon work supported by the National Science Foundation (Grant No. CHE-0715268) and by the donors of the American Chemical Society Petroleum Research Fund (Grant No. 44262-AC6). The Center for Computational Molecular Science and Technology is funded through an NSF CRIF award (CHE 04-43564) and by Georgia Tech.

Supporting Information Available: Parallel-displaced potential energy curves and Cartesian coordinates for minimum energy geometries. This material is available free of charge via the Internet at http://pubs.acs.org.

References and Notes

(1) Meyer, E. A.; Castellano, R. K.; Diederich, F. *Angew. Chem., Int. Ed.* **2003**, *42*, 1210.
(2) Burley, S. K.; Petsko, G. A. *Science* **1985**, *229*, 23.
(3) Saenger, W. *Principles of Nucleic Acid Structure*; Springer-Verlag: New York, 1984.
(4) Collings, J. C.; Roscoe, K. P.; Robins, E. G.; Batsanov, A. S.; Stimson, L. M.; Howard, J. A. K.; Clark, S. J.; Marder, T. B. *New J. Chem.* **2002**, *26*, 1740.
(5) Ringer, A. L.; Sherrill, C. D. *Chem. Eur. J.* **2008**, *14*, 2542.
(6) Jaffe, R. L.; Smith, G. D. *J. Chem. Phys.* **1996**, *105*, 2780.
(7) Hobza, P.; Selzle, H. L.; Schlag, E. W. *J. Phys. Chem.* **1996**, *100*, 18790.
(8) Tsuzuki, S.; Uchimaru, T.; Matsumura, K.; Mikami, M.; Tanabe, K. *Chem. Phys. Lett.* **2000**, *319*, 547.
(9) Špirko, V.; Engkvist, O.; Soldán, P.; Selzle, H. L.; Schlag, E. W.; Hobza, P. *J. Chem. Phys.* **1999**, *111*, 572.
(10) Tsuzuki, S.; Honda, K.; Uchimaru, T.; Mikami, M.; Tanabe, K. *J. Am. Chem. Soc.* **2002**, *124*, 104.
(11) Tsuzuki, S.; Uchimaru, T.; Sugawara, K.; Mikami, M. *J. Chem. Phys.* **2002**, *117*, 11216.
(12) Sinnokrot, M. O.; Sherrill, C. D. *J. Phys. Chem. A* **2006**, *110*, 10656.
(13) Sinnokrot, M. O.; Sherrill, C. D. *J. Phys. Chem. A* **2004**, *108*, 10200.
(14) Sinnokrot, M. O.; Valeev, E. F.; Sherrill, C. D. *J. Am. Chem. Soc.* **2002**, *124*, 10887.
(15) Carver, F. J.; Hunter, C. A.; Livingstone, D. J.; McCabe, J. F.; Seward, E. M. *Chem. Eur. J.* **2002**, *8*, 2848.
(16) Adams, H.; Carver, F. J.; Hunter, C. A.; Morales, J. C.; Seward, E. M. *Angew. Chem., Int. Ed. Engl.* **1996**, *35*, 1542.
(17) Ringer, A. L.; Sinnokrot, M. O.; Lively, R. P.; Sherrill, C. D. *Chem. Eur. J.* **2006**, *12*, 3821.
(18) Lee, E. C.; Hong, B. H.; Lee, J. Y.; Kim, J. C.; Kim, D.; Kim, Y.; Tarakeshwar, P.; Kim, K. S. *J. Am. Chem. Soc.* **2005**, *127*, 4530.
(19) Sinnokrot, M. O.; Sherrill, C. D. *J. Am. Chem. Soc.* **2004**, *126*, 7690.
(20) Sinnokrot, M. O.; Sherrill, C. D. *J. Phys. Chem. A* **2003**, *107*, 8377.
(21) Pluháčková, K.; Jurečka, P.; Hobza, P. *Phys. Chem. Chem. Phys.* **2007**, *9*, 755.
(22) Riley, K. E.; Merz, K. M. *J. Phys. Chem. B* **2005**, *109*, 17752.
(23) Paliwal, S.; Geib, S.; Wilcox, C. S. *J. Am. Chem. Soc.* **1994**, *116*, 4497.
(24) Kim, E.; Paliwal, S.; Wilcox, C. S. *J. Am. Chem. Soc.* **1998**, *120*, 11192.
(25) Cozzi, F.; Ponzini, F.; Annunziata, R.; Cinquini, M.; Siegel, J. S. *Angew. Chem., Int. Ed. Engl.* **1995**, *34*, 1019.
(26) Cozzi, F.; Cinquini, M.; Annuziata, R.; Dwyer, T.; Siegel, J. S. *J. Am. Chem. Soc.* **1992**, *114*, 5729.
(27) Cozzi, F.; Siegel, J. S. *Pure Appl. Chem.* **1995**, *67*, 683.
(28) Cockroft, S. L.; Perkins, J.; Zonta, C.; Adams, H.; Spey, S. E.; Low, C. M. R.; Vinter, J. G.; Lawson, K. R.; Urch, C. J.; Hunter, C. A. *Org. Biomol. Chem.* **2007**, *5*, 1062.

(29) Cockroft, S. L.; Hunter, C. A.; Lawson, K. R.; Perkins, J.; Urch, C. J. *J. Am. Chem. Soc.* **2005**, *127*, 8594.
(30) Rashkin, M. J.; Waters, M. L. *J. Am. Chem. Soc.* **2002**, *124*, 1860.
(31) Lee, E. C.; Kim, D.; Jurečka, P.; Tarakeshwar, P.; Hobza, P.; Kim, K. S. *J. Phys. Chem. A* **2007**, *111*, 3446.
(32) Gung, B. W.; Amicangelo, J. C. *J. Org. Chem.* **2006**, *71*, 9261.
(33) Tsuzuki, S.; Honda, K.; Uchimaru, T.; Mikami, M. *J. Chem. Phys.* **2006**, *125*, 124304.
(34) Shieh, H.-S.; Berman, H. M.; Dabrow, M.; Neidle, S. *Nucleic Acids Res.* **1980**, *8*, 85.
(35) Itahara, T.; Imaizumi, K. *J. Phys. Chem. B* **2007**, *111*, 2025.
(36) Megiel, E.; Kasprzycka-Guttman, T.; Jagielska, A.; Wroblewska, L. *J. Mol. Struct.* **2001**, *569*, 111.
(37) Piacenza, M.; Grimme, S. *Chem. Phys. Chem.* **2005**, *6*, 1554.
(38) Mishra, B. K.; Sathyamurthy, N. *J. Phys. Chem. A* **2005**, *109*, 6.
(39) Mignon, P.; Loverix, S.; Proft, F. D.; Geerlings, P. *J. Phys. Chem. A* **2004**, *108*, 6038.
(40) Tsuzuki, S.; Mikami, M.; Yamada, S. *J. Am. Chem. Soc.* **2007**, *129*, 8656.
(41) Bates, D. M.; Anderson, J. A.; Oloyede, P.; Tschumper, G. S. *Phys. Chem. Chem. Phys.* **2008**, *10*, 2775.
(42) Wang, W.; Hobza, P. *Chem. Phys. Chem.* **2008**, *9*, 1003.
(43) Jeziorski, B.; Moszynski, R.; Szalewicz, K. *Chem. Rev.* **1994**, *94*, 1887.
(44) Williams, H. L.; Szalewicz, K.; Jeziorski, B.; Moszynski, R.; Rybak, S. *J. Chem. Phys.* **1993**, *98*, 1279.
(45) Raghavachari, K.; Trucks, G. W.; Pople, J. A.; Head-Gordon, M. *Chem. Phys. Lett.* **1989**, *157*, 479.
(46) Dunning, T. H. *J. Chem. Phys.* **1989**, *90*, 1007.
(47) Kendall, R. A.; Dunning, T. H.; Harrison, R. J. *J. Chem. Phys.* **1992**, *96*, 6796.
(48) Grimme, S. *J. Chem. Phys.* **2003**, *118*, 9095.
(49) Gauss, J.; Stanton, J. F. *J. Phys. Chem. A* **2000**, *104*, 2865.
(50) Innes, K. K.; Ross, I. G.; Moomaw, W. R. *J. Mol. Spectrosc.* **1988**, *132*, 492.
(51) Takatani, T.; Hohenstein, E. G.; Sherrill, C. D. Manuscript in preparation.
(52) Boys, S. F.; Bernardi, F. *Mol. Phys.* **1970**, *19*, 553.
(53) Janowski, T.; Pulay, P. *Chem. Phys. Lett.* **2007**, *447*, 27.
(54) Halkier, A.; Klopper, W.; Helgaker, T.; Jørgensen, P.; Taylor, P. R. *J. Chem. Phys.* **1999**, *111*, 9157.
(55) Crawford, T. D.; Sherrill, C. D.; Valeev, E. F.; Fermann, J. T.; King, R. A.; Leininger, M. L.; Brown, S. T.; Janssen, C. L.; Seidl, E. T.; Kenny, J. P.; Allen, W. D. *J. Comput. Chem.* **2007**, *28*, 1610.
(56) Werner, H.-J.; Knowles, P. J.; Lindh, R.; Manby, F. R.; Schütz, M.; Celani, P.; Korona, T.; Rauhut, G.; Amos, R. D.; Bernhardsson, A.; Berning, A.; Cooper, D. L.; Deegan, M. J. O.; Dobbyn, A. J.; Eckert, F.; Hampel, C.; Hetzer, G.; Lloyd, A. W.; McNicholas, S. J.; Meyer, W.; Mura, M. E.; Nicklass, A.; Palmieri, P.; Pitzer, R.; Schumann, U.; Stoll, H.; Stone, A. J.; Tarroni, R.; Thorsteinsson, T. *Molpro*, version 2006.1, a package of ab initio programs, 2006; see http://www.molpro.net.
(57) *Jaguar 5.5*; Schrodinger, LLC, Portland, OR, 2003.
(58) Bukowski, R.; Cencek, W.; Jankowski, P.; Jeziorski, B.; Jeziorska, M.; Kucharski, S. A.; Lotrich, V. F.; Misquitta, A. J.; Moszynski, R.; Patkowski, K.; Rybak, S.; Szalewicz, K.; Williams, H. L.; Wheatley, R. J.; Wormer, P. E. S.; Zuchowski, P. S. *SAPT2006*: An ab initio program for many-body symmetry-adapted perturbation theory calculations of intermolecular interaction energies; see: http://www.physics.udel.edu/~szalewic/SAPT.
(59) Hill, J. G.; Platts, J. A. *J. Chem. Theory Comput.* **2007**, *3*, 80.
(60) Doerksen, R. J.; Thakkar, A. J. *Int. J. Quantum Chem. Symp.* **1996**, *30*, 1633.

JP809062X